Structure and photochemical behaviour of 3-azido-acrylophenones: a matrix isolation infrared spectroscopy study

Susy Lopes [a], Cláudio M. Nunes [a], Andrea Gómez-Zavaglia [a,b], Teresa M.V.D. Pinho e Melo [a,*], Rui Fausto [a,*]

[a] Department of Chemistry, University of Coimbra, P-3004-535 Coimbra, Portugal
[b] Centro de Investigación y Desarrollo en Criotecnología de Alimentos (Conicet La Plata, UNLP), RA-1900, Argentina

ARTICLE INFO

ABSTRACT

(Z)-3-Azido-3-methoxycarbonyl-2-chloro-acrylophenone (MACBP) has been synthesized, isolated in low temperature argon and xenon matrices and studied by FTIR spectroscopy, complemented by DFT(B3LYP)/6-311++G(d,p) calculations. The molecule was characterized both structurally and spectroscopically, and its photochemistry used to probe the mechanism of photo-induced conversion of 3-azido-acrylophenones into oxazoles. In situ UV irradiation ($\lambda = 235$ nm) of matrix-isolated MACBP yielded as primary photoproduct a 2H-azirine, which undergoes subsequent photoisomerization to methyl 4-chloro-5-phenyl-1,3-oxazole-2-carboxylate. In a competitive process, a ketenimine is also formed upon photolysis of MACBP. The reported results indicate that this ketenimine must be formed from the starting 3-azido-acrylophenone via a Curtius type concerted rearrangement.

© 2011 Elsevier Ltd. All rights reserved.

1. Introduction

Molecules containing the azido-moiety ($-N_3$) are energy-rich and flexible chemical systems that have enjoyed increased interest over the years. Organic azides constitute a versatile class of compounds used as building blocks in organic synthesis,[1–5] with particular relevance in peptide and bioorganic chemistry.[6–14] The copper(I)-catalyzed Huisgen azide–alkyne 1,3-dipolar cycloaddition forming triazoles,[7,10,11,14–20] known as the 'click reaction', is one of the most effective ways to make connections between structures that bear a wide variety of functional groups. This reaction has found applications in a wide variety of research areas, for example, in materials science and drug design.[10,11,14]

It is well known that azides are also explosive substances that decompose with the release of nitrogen through the slightest input of external energy.[4] However, in spite of their explosive properties, the industrial interest in organic azide compounds extends to a number of areas, as they have applications in polymer synthesis[9,13,16,17] and light-induced activation of polymer surfaces,[21,22] as photo resistors for lithography,[23,24] in photo affinity labeling biological methods,[25,26] or as energetic additives for solid propellants.[27,28]

The mechanisms for the decomposition of azides through thermal and/or photochemical treatment and the intermediates formed have been extensively investigated. Nevertheless, there are still many cases where general consensus in relation to the precise mechanism involved in these processes could not been obtained. For example, it is considered that, in general, the release of molecular nitrogen is accompanied by the formation of a nitrene intermediate, which then undergoes further reactions, including isomerization to ketenimines, cyclization to azirines, C–H bond insertion or C=C bond addition.[29–39] However, even in the case of the common synthetic approach for preparing 2H-azirines from photolysis or thermolysis of vinyl azides the precise mechanism of the reaction has been questioned, in particular in relation to the involvement of the nitrene intermediate in the process (vs concerted rearrangement).[32–39]

Recently,[40] we reported that the thermolysis of 3-azido-3-methoxycarbonyl-2-halo-acrylophenones (e.g., 1, in Scheme 1) produces the corresponding 2-benzoyl-2-halo-2H-azirine-3-carboxylates (e.g., 2), which undergo ring expansion to give 4-halo-5-phenyl-1,3-oxazole-2-carboxylates (e.g., 6) and not the isomeric isoxazoles (e.g., 4). Since oxazoles are obtained in high yield (>90%) we could conclude that only the reaction pathway B is observed. In fact, the formation of the vinylnitrene intermediates (e.g., 3) should lead to the competitive formation of the corresponding isoxazoles. It

* Corresponding authors. E-mail addresses: tmelo@ci.uc.pt (T.M.V.D. Pinho e Melo), rfausto@ci.uc.pt (R. Fausto).

should be emphasized that the stereochemistry of the 3-azido-acrylophenones (the structure of the bromo derivative was established as *Z* using X-ray crystallography,[41] bearing the azide and benzoyl groups *trans*) precludes their direct conversion into isoxazoles by a concerted process. However, the formation of 2-benzoyl-2*H*-azirines from the vinyl azides in a concerted manner is possible. The production of the oxazole via nitrile ylide intermediates was initially not expected,[41] since it is generally accepted that 2*H*-azirines react preferentially upon thermal excitation through cleavage of the C–N bond, the required route to the nitrene species,[42–51] whereas thermal cleavage of the C–C bond is less common.[45]

Scheme 1.
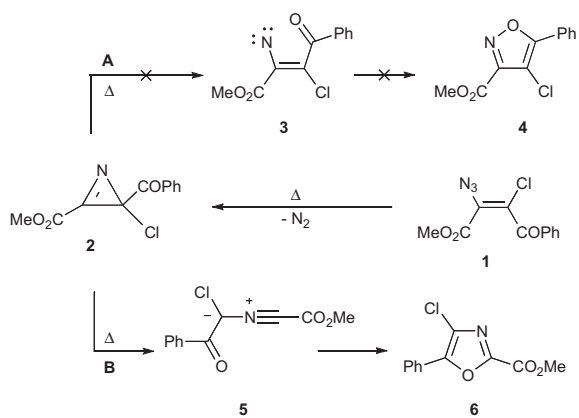
On the other hand, photochemical excitation of 2*H*-azirines leads most frequently to the C–C bond cleavage of the azirine ring, yielding the corresponding nitrile ylides (e.g., **5**),[46–53] which are the expected intermediates to the oxazole production. However, photochemical processes involving cleavage of the C–N bond have also been observed upon photolysis of substituted azirines bearing electron-withdrawing substituents in the ring.[48–51,54,55]

In the present study, (*Z*)-3-azido-3-methoxycarbonyl-2-chloro-acrylophenone (**1**) (or methyl (*Z*)-2-azido-3-chloro-3-benzoylpropenoate, MACBP; Fig. 1) has been chosen as target to further investigation of the mechanism of conversion of 3-azido-acrylophenones into oxazoles. The compound was synthesized and then isolated in cryogenic matrices (Ar, Xe), where its conformational preferences and UV-induced photochemistry were investigated by infrared spectroscopy, supported by DFT calculations. The matrix isolation technique was selected to carry out this study because in a matrix the reactions are cage-confined, since molecular diffusion is inhibited, and no reactions involving molecules initially located in different matrix sites can occur. Hence, only unimolecular reactions are expected to take place in relation with the molecule of the initial reactant, a characteristic that introduces a very useful simplification in the study of photochemical reactivity, in particular in the characterization of the associated reaction mechanisms.

As it will be shown in detail in this paper, upon photolysis (λ >235 nm) matrix-isolated **1** (MACBP) evolves to the corresponding azirine **2** (MBCAC), which subsequently undergoes ring expansion to the oxazole **6** (MCPOC). An additional photoproduct, *C*-chloro-*C*-benzoyl-*N*-methoxycarbonylketenimine **7** (CBMK) was also observed. It is proposed that it results from a Curtius type concerted rearrangement of the starting 3-azido-acrylophenone **1**, since the alternative pathway involving the initial formation of the 2*H*-azirine would require the generation of vinyl nitrene **3**. The expected vinyl nitrene cyclization product, the corresponding isoxazole, was not observed, which supports the conclusion that the nitrene species is not involved in this conversion.
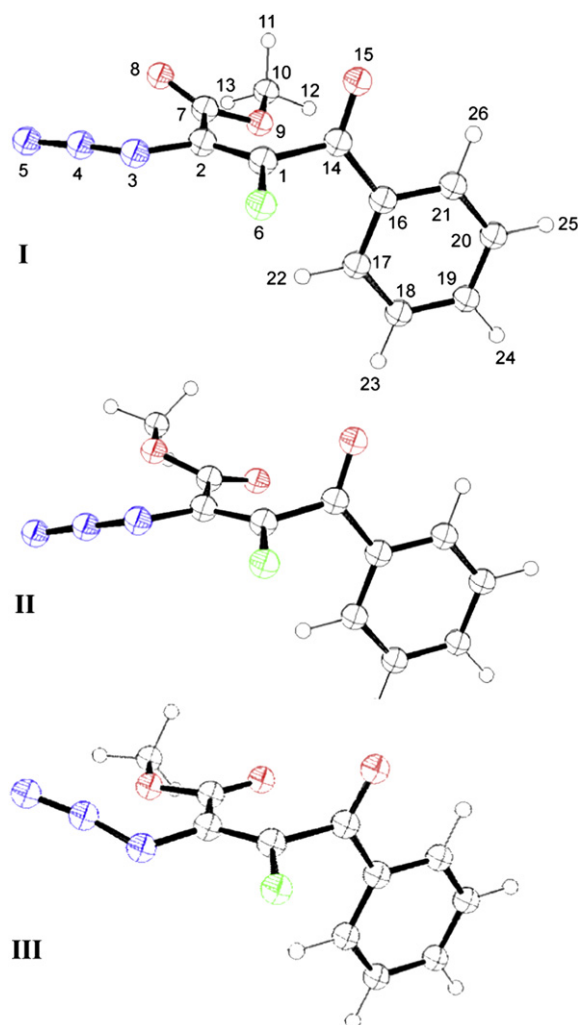
Fig. 1. Low energy conformers of **1** (MACBP), optimized at the DFT(B3LYP)/6-311++G(d,p) level of theory, with atom numbering. The picture was made using the Ortep-3 for Windows program (Farrugia, L. J. *J. Appl. Cryst.* 1997, *30*, 565). Atoms color code: carbon, hydrogen: black; nitrogen: blue; chlorine: green; oxygen, red.

2. Computational methods

A systematic preliminary conformational exploration of the MACBP potential energy surface (PES) was performed using the semi-empirical PM3 method[56,57] and the HyperChem Conformational Search module (CyberChem, Inc.© 2004).[58] These calculations provided a quick assessment of the main features of the conformational space of the molecule, which were later on taken into account in the subsequent analysis performed at higher level of theory. Taking into account the high flexibility of the MACBP molecule, a random search appeared as the most appropriate way to perform the conformational search.[59–61] The program generates starting conformations for energy minimization using a random variation of the conformationally relevant dihedral angles obtained for previously located minima.[60,61] The method searches on until no new minima are generated. The same approach was used in the structural studies performed for the conformationally flexible photoproducts of MACBP, specifically the azirine (MBCAC), and ketenimine (CBMK) photoproducts. For all three compounds 30,000 initial structures were generated by varying the relevant dihedral angles, and the structures corresponding to the 25 (18 for CBMK) lowest energy unique minima were saved and used as input geometries for the subsequent higher level calculations undertaken with Gaussian 03[62] at the DFT level of theory, using the split

valence triple-ζ 6-311++G(d,p) basis set[63] and the three-parameter B3LYP density functional.[64,65] Structures were optimized using the Geometry Direct Inversion of the Iterative Subspace (GDIIS) method.[66,67] Transition states for conformational interconversions were determined at the same level of approximation, with help of the synchronous transit-guided quasi-Newton (STQN) method.[68]

In order to assist the analysis of the experimental infrared (IR) spectra, vibrational frequencies and IR intensities were also calculated at the same level of theory. The computed harmonic frequencies were scaled down by a single factor (0.978) to correct them for the effects of basis set limitations, neglected part of electron correlation and anharmonicity effects. The nature of stationary points on the potential energy surface was checked through the analysis of the corresponding Hessian matrix.

Normal coordinate analysis was undertaken in the internal coordinates space, as described by Schachtschneider and Mortimer[69] and the optimized geometries and harmonic force constants resulting from the DFT(B3LYP)/6-311++G(d,p) calculations. The internal coordinates used in this analysis were defined following the recommendations of Pulay et al.[70]

3. Results and discussion

3.1. Molecular structures and relative energies of MACBP conformers

MACBP has four conformationally relevant rotational axes defined by the $N_4=N_3-C_2=C_1$, $O_8=C_7-C_2=C_1$, $C_{16}-C_{14}-C_1=C_2$, and $C_{17}-C_{16}-C_{14}-C_1$ dihedral angles. The s-cis conformation of a methyl ester group ($C_{10}-O_9-C_7=O_8$ equal to $\sim 0°$) is well-known[71–73] to be considerably more stable than the s-trans one ($C_{10}-O_9-C_7=O_8$ equal to $\sim 180°$) and only structures with the first type of arrangement were taken into account (s-trans methyl ester minima can be expected to be at least 25 kJ mol^{-1} higher in energy than the s-cis forms[71–73]). After re-optimizing at the DFT(B3LYP)/6-311++G(d,p) level of theory the structures obtained from the preliminary semi-empirical random conformational search, 14 different minima were found on the PES of the molecule with relative energies within 19 kJ mol^{-1}. These minima correspond to seven pairs of equivalent-by-symmetry conformers, all of them belonging to the C_1 symmetry point group. Table 1 displays the predicted relative energies (including zero-point corrections) of these conformers.

The calculated optimized geometries for the three most stable conformers are given in Table S1 (Supplementary data). In the description of the structures of the conformers, the position of the azide ($-N=N\equiv N$), carboxylic ester ($-COOCH_3$) and benzoyl ($-C_6H_5C=O$) groups will be considered in relation to the central $C_1=C_2$ double bond.

Rotation around the N_3-C_2 bond defines the relative orientation of the azide group in relation to the $C_2=C_1$ double bond. The calculations show that the orientation of the azide moiety allows us to divide the conformers into two groups: one where the azide is in an almost trans orientation, to which the three lower energy conformers belong (I, II, and III, where the $N_4=N_3-C_2=C_1$ dihedral angle is $-171.0°$, -160.1, and $+155°$, respectively), and the other where the azide in a nearly cis orientation ($N_4=N_3-C_2=C_1$ dihedral angle of ca. $\pm 40°$), to which the higher energy conformers (IV–VII) belong. The higher energy of conformers IV–VII can then be associated with unfavorable interactions between the closely located azide and chlorine substituents in these forms.

The carboxylic ester group can be arranged in a cis ($O_8=C_7-C_2=C_1 \sim 0°$) or trans ($O_8=C_7-C_2=C_1 \sim 180°$) orientation towards the central double bond, while the benzoyl group exhibits a quasi-planar configuration and assumes a nearly perpendicular geometry in relation to the main molecular plane in all conformers. Among the three most stable conformers (see Fig. 1), conformer I presents the unique arrangement of its carboxylic ester in the trans orientation relative to the $C_2=C_1$ bond, while in II and III this group adopts the cis arrangement. For the higher energy conformers, the carboxylic ester group is cis in conformers IV and VI and trans in conformers V and VII.

According to calculations, repulsive interactions between the azide and carboxylic ester groups should be considered the main factor determining the relative stability of the three lower energy conformers of MACBP. In conformer I, it is the carbonyl oxygen (O_8), which interacts with the azide group, whereas in conformers II and III the interaction involves the methoxyl oxygen atom (O_9). The calculated atomic polar tensor (APT) charges[74] for the three conformers are shown in Table 2. From this table, it can be noticed that O_9 is more negatively charged than O_8, so that the $N_3 \cdots O_9$ electrostatic repulsion in II and III is more important than the $N_3 \cdots O_8$ electrostatic repulsion in I. In addition, the $N_3 \cdots O_{8/9}$ contact distances decrease in the order I (285.8 pm) > II (276.7 pm) > III (275.5 pm), also contributing to make the $N_3 \cdots O_{8/9}$ repulsive electrostatic interaction more important in the order III>II>I.

Table 1
DFT(B3LYP)/6-311++G(D,P) calculated relative energies (ΔE_0/kJ mol^{-1}), including zero-point vibrational contributions, and predicted relative populations for the conformers of MACBP

Conformer [a]	ΔE_0	Population (%)	
		$T=298$ K	$T=323$ K
I	0.00	75.3	72.4
II	3.95	15.3	16.6
III	5.40	8.5	9.7
IV	12.73	0.4	0.6
V	14.07	0.3	0.4
VI	15.26	0.2	0.2
VII	18.71	~ 0.0	0.1

[a] See Fig. 1 and Fig. S1 (Supplementary data) for structures of the conformers.

According to the calculations, conformers II and III are 3.95 and 5.40 kJ mol^{-1} higher in energy than the most stable conformer I (Fig. 1). The remaining forms (conformers IV–VII; Fig. S1 in the Supplementary data) have calculated relative energies at least 12 kJ mol^{-1} higher than that of conformer I, and as a whole are predicted to constitute less than 1.0% of the total conformational population in gas phase at room temperature (see Table 1).

Table 2
DFT(B3LYP)/6−311++G(D,P) calculated atomic polar tensor (APT) charges on atoms (with hydrogens summed into heavy atoms) for conformers I, II, and III of MACBP[a]

Atom	APT charges/e		
	I	II	III
C_1	0.117	0.182	0.218
C_2	0.249	0.205	0.176
N_3	−0.905	−0.883	−0.882
N_4	1.164	1.127	1.130
N_5	−0.618	−0.617	−0.616
Cl_6	−0.314	−0.304	−0.298
C_7	1.196	1.236	1.233
O_8	−0.746	−0.715	−0.729
O_9	−0.818	−0.911	−0.897
C_{10}	0.465	0.483	0.482
C_{14}	1.208	1.210	1.192
O_{15}	−0.789	−0.800	−0.798
C_{16}	−0.339	−0.342	−0.332
C_{17}	0.068	0.110	0.103
C_{18}	−0.051	−0.052	−0.046
C_{19}	0.061	0.061	0.058
C_{20}	−0.052	−0.055	−0.052
C_{21}	0.104	0.065	0.058

[a] See Fig. 1 for atom numbering. 1 e=1.60217646×10^{-19} °C.

It is interesting to point out that the crystal structure determined by X-ray diffraction of the analogous bromo-substituted compound, methyl (*Z*)-2-azido-3-bromo-3-benzoyl-propenoate[41] bears great similarity to the second stable conformer (**II**) of MACBP. In the bromo-substituted molecule, the $N_4=N_3-C_2=C_1$, $O_8=C_7-C_2=C_1$ and $C_{16}-C_{14}-C_1=C_2$ dihedral angles were found to be $-162.7(6)°$, $14.4(10)°$, and $-102.0(10)°$, which can be compared with the values for the same dihedral angles calculated for conformer **II** of MACBP ($-160.1°$, $19.6°$, and $-106.6°$, respectively).

3.2. Matrix isolation infrared spectra of as-deposited matrices

As shown in the previous section, the calculations predicted three experimentally relevant conformers of MACBP in gas phase: conformers **I**, **II** and **III**, with estimated relative energies of 0.0, 3.95 and 5.40 kJ mol^{-1}, respectively. At the sublimation temperature used to prepare the cryogenic matrices ($T=323$ K) the estimated gas phase equilibrium Boltzmann populations are 72.4%, 16.6%, and 9.7% (see Table 1). The combined populations of the higher energy conformers (**IV**–**VII**) are 1.3% and therefore these forms are of no practical interest for our study.

Another important piece of information for interpretation of the matrix-isolation experimental spectroscopic results described in this section is the knowledge of the energy barriers for interconversion between the conformers whose abundance in the gas phase prior to deposition is significant. This is because when a higher energy conformer is separated from a lower energy form by a small barrier (of a few kJ mol^{-1}) the higher energy form can be converted into the lower energy form during matrix deposition, since the thermal energy available in the gaseous beam might be enough to allow surpassing of the barrier during the landing of the molecules onto the cold substrate of the cryostat (conformational cooling effect[51,75,76–80]). The energy barrier between **III**→**II** was indeed found to be extremely low, amounting only to ca. 0.03 kJ mol^{-1} (1.4 kJ mol^{-1} in the opposite direction), indicating that conformer **III** shall relax into conformer **II** during matrix deposition. On the other hand, the energy barrier separating forms **I** and **II** is ~15 kJ mol^{-1} (for **II**→**I**; ca. 19 kJ mol^{-1} in the reverse direction). With an energy barrier of this magnitude, the **II**→**I** conversion cannot occur during deposition of the matrices at the deposition temperatures used (10–20 K),[51,75,76–80] so that we can expect experimental observation of both conformers **I** and **II** in the matrices, the latter with a population equal to the sum of the populations of conformers **II** and **III** in the gas phase before deposition. The expected **I**:**II** population ratio in the matrices is then 72.4:26.3, i.e., nearly 3:1.

Fig. 2 shows the infrared spectra of MACBP isolated in both solid argon and xenon (as-deposited matrices; nozzle temperature 50 °C, substrate temperature: argon, 10 K, xenon, 20 K), together with the calculated spectra for conformers **I** and **II** and the simulated spectrum of the predicted conformational mixture in the matrices assuming the relative abundances equal to 72.4:26.3 (calculated infrared spectrum of conformer **III** is included in the Supplementary data; Fig. S2). In the simulated spectra, bands were represented by Lorentzian functions centered at the calculated wavenumbers (scaled by 0.978) and with fwhm (full width at half maximum) equal to 2 cm^{-1} (see Experimental section for methodology used in the matrix isolation experiments).

The spectra obtained in argon and xenon matrices look very similar and they are generally well reproduced by the simulated spectrum. The proposed assignments for the fundamental bands are given in Table 3. MACBP has 72 fundamental vibrations, all of them active in the infrared. The definition of the internal coordinates adopted in the performed vibrational analysis is provided in Table S2 (Supplementary data). The calculated wavenumbers, infrared intensities, and potential energy distributions resulting
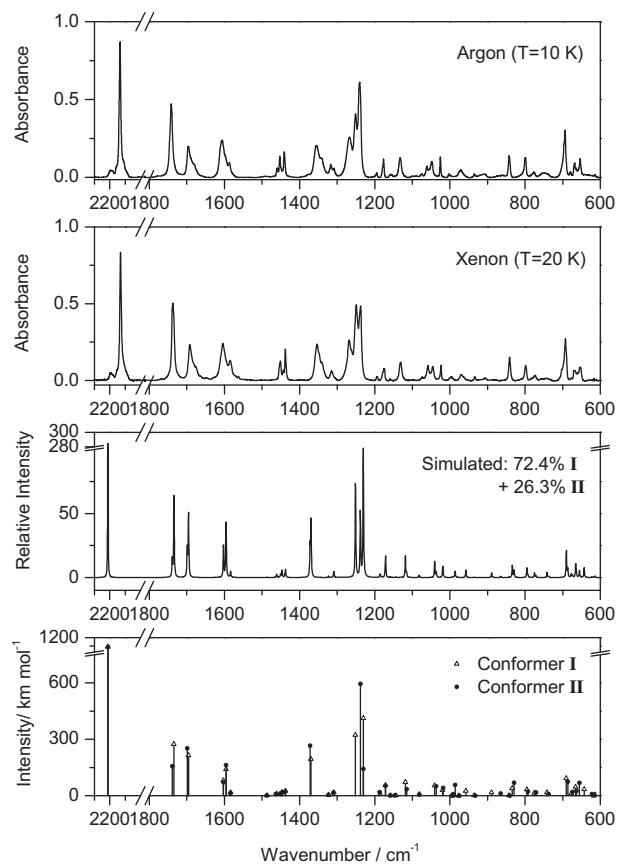

Fig. 2. *Top* (two panels): infrared spectra of MACBP isolated in solid argon and xenon (as-deposited matrices; temperature of the deposited vapor: 323 K; substrate temperature during deposition: argon, 10 K, xenon, 20 K); *Bottom*: DFT(B3LYP)/6-311++G(d,p) calculated infrared spectra of MACBP conformers shown as stick spectra (wavenumbers scaled by 0.978): **I** (open triangles, △) and **II** (black circles, ●); *Middle*: simulated spectrum of the expected gas phase equilibrium conformational mixture at 323 K, built by adding the calculated spectrum of conformers **I** and **II** with intensities scaled by their predicted populations (72.4% for conformer **I** and 26.3% for conformer **II**; see text). In the simulated spectra, bands were represented by Lorentzian functions centered at the calculated wavenumbers (scaled by 0.978) and with fwhm (full width at half maximum) equal to 2 cm^{-1}.

from normal mode analysis carried out for the three MACBP conformers are presented in Tables S3–S5 (Supplementary data).

Due to the similarity of the spectra of the two experimentally relevant conformers (**I** and **II**), secure assignment of bands to a unique conformer is not possible, except in the 1270–1230 cm^{-1} spectral range, where the calculations predict a different pattern for the spectral profile of the two forms (see Fig. 2). Besides the azide anti-symmetric stretching band observed as an intense band at ~2130 cm^{-1} (both in argon and xenon), the bands in the 1270–1230 cm^{-1} range are the most intense of the spectra. These bands are due to the νC–O ester (also with some contribution from the stretching of the adjacent C–C bond; notated as νC–C$_\alpha$ E in Table 3) and νC$_{14}$–C$_{16}$ (designated as νC–C$_{Ph}$ in Table 3) stretching modes. The higher frequency band, observed in argon matrix at 1267/1261 cm^{-1} (1268/1262 cm^{-1} in xenon) is due to the ester νC–O stretching in conformer **I**, which is predicted to occur at 1251 cm^{-1} with an intensity of 324.0 km mol^{-1} by the calculations. The middle band observed in this region (1251 cm^{-1} in argon and 1249 cm^{-1} in xenon) is due to the same mode in conformer **II**, where it is predicted by the calculations to occur at 1238 cm^{-1} with an intensity of 595.2 km mol^{-1}. The lower frequency band (1240 cm^{-1} in argon; 1237 cm^{-1} in xenon) results from the absorption of the νC$_{14}$–C$_{16}$ stretching mode in the two conformers. This last vibration is predicted at 1231 cm^{-1} with an intensity of

Table 3
Experimental (matrix-isolation) and calculated vibrational data for MACBP with vibrational assignments based on the results of normal coordinate analysis[a]

Experimental		Calculated				
Ar matrix	Xe matrix	Conformer **I**		Conformer **II**		Approximate description[b]
ν	ν	ν	I_{IR}	ν	I_{IR}	
3109	3101	3129	7.8	3131	7.2	ν(C–H5); ν(C–H1)
3095/3093	3087	3124	7.4	3123	8.6	ν(C–H1); ν(C–H4)
3074/3068	3064	3115	15.5	3115	18.2	ν(C–H4); ν(C–H5)
3042	3037	3107	5.6	3107	5.5	ν(C–H2)
3038	3030	3100	6.9	3100	8.5	νCH$_3$ as′
		3097	0.1	3097	0.2	ν(C–H3)
3021/3012	3001	3067	10.0	3067	11.2	νCH$_3$ as″
2967/2964	2951	2991	24.1	2991	25.2	νCH$_3$ s
2158/2134/2109	2153/2130	2213	981.7	2212	972.7	ν(N=N) as
1746 sh/1742/1740	1739/1737/1735 sh	1734	274.2	1739	156.0	ν(C=O) E
1697/1689/1679	1692/1684/1676	1696	214.9	1699	252.4	ν(C=O) Ph
1611/1607	1610	1603	81.2	1603	71.2	νPh3
1605/1597	1604	1596	140.3	1595	162.4	ν(C=C)
1589/1586	1585/1582	1583	16.5	1584	14.7	νPh4
1492	1491	1486	0.8	1487	0.9	δ(C–H2)
1461 (**II**); 1459 (**I**)	1455/1453 (**II**) 1451 (**I**)	1461	10.6	1463	8.7	δCH$_3$ as′
1453/1449	1443	1451	7.5	1451	10.8	δCH$_3$ as″
		1447	18.3	1447	16.8	νPh6,δ(C–H3)
1442/1441/1439 sh	1438/1436 sh	1437	25.2	1439	21.5	δCH$_3$ s
1356/1341	1353/1348/1341	1370	194.6	1372	265.6	ν(N=N) s
1317/1315	1315	1323	3.5	1323	3.8	δ(C–H1)
1311/1307	1311	1309	17.2	1310	16.3	νPh2
1267/1261 (**I**); 1251 (**II**)	1268/1262 (**I**); 1249 (**II**)	1251	324.0	1238	595.2	ν(C–O), ν(C–C$_\alpha$) E
1240	1237	1231	413.1	1230	141.9	ν(C–C $_{Ph}$)
1194	1194/1192	1185	8.5	1186	18.9	γCH$_3$′
1180/1177	1178/1175/1174	1171	55.2	1172	52.4	δ(C–H4)
1158/1156/1155	1159	1159	1.5	1158	1.0	δ(C–H5)
.	.	1144	1.7	1147	0.9	γCH$_3$″
1132	1131	1119	72.5	1115	33.5	ν(C–O), ν(O–CH$_3$)
1074	1073	1082	6.7	1082	5.5	νPh6
1061 (**I**); 1047 (**II**)	1059 (**I**); 1045 (**II**)	1041	53.7	1036	50.5	νPh5, ν(C–C)
1026	1023	1019	29.2	1018	40.6	νPh1
		994	1.1	994	1.1	δPh1
1002/998	1000/996	992	0.1	990	8.6	γ(C–H5)
		977	0.6	975	0.2	γ(C–H4)
		–	–	986	57.4	ν(O–CH$_3$)
975/971 (**I**)	969/962 (**I**)	958	26.1	–	–	ν(O–CH$_3$)
935	934	935	1.3	933	0.2	γ(C–H3)
918 (**I**); 906 (**II**)	910 (**I**); 906 (**II**)	889	16.5	865	12.1	ν(C–Cl)
842	841	843	0.8	841	0.5	γ(C–H2)
		834	40.1	829	67.7	δ(C=O), ν(C–N); ν(C–N)
799/798	798/796	795	33.1	792	20.7	γ(C=O)
783/776	780/773	775	15.4	771	17.6	γ(C=O) E
746	746	742	17.3	737	8.5	γ(C=O) E, δ(OCO); γ(C=O) E, ν(C–Cl)
702/697/693	702/692/689	690	91.9	686	74.4	γ(C–H1)
679	677	677	11.9	674	20.6	τPh1
668/665/663	670/666/662	665	46.3	664	25.4	δPh3; δ(NNN), δ(OCO)
659 (**II**)	660/659 (**II**)	–	–	655	68.6	δ(NNN)
653 (**I**)	653 (**I**)	643	33.7	–	–	δPh3
621	622	617	0.4	622	8.1	δPh2; δ(CCC$_{Ph}$), γ(C–Cl)
614/610	613/610	614	5.1	616	2.4	γ(C–Cl); δPh2
530	526	516	4.0	522	7.5	ν(NNN)

[a] Wavenumbers (cm^{-1} scaled by 0.978), calculated intensities (km mol^{-1}). [b] In the approximate description, the symbol ';' separates the description for **I** and **II**, when they are different, while ',' indicates that the approximate description for a given mode has more than one relevant contributing coordinate; ν, bond stretching, δ, bending, γ, rocking, τ, torsion, s, symmetric, as, asymmetric, Ph, phenyl ring, E, ester; sh, shoulder, n.obs., not observed. See Table S2 (Supplementary data) for definition of internal coordinates and Tables S3 and S4 (Supplementary data) for potential energy distributions.

413.1 km mol^{-1} in form **I**, and at 1230 cm^{-1} with an intensity of 141.9 km mol^{-1} in form **II**, so that the predominant contribution to the band is due to conformer **I**.

The different profiles of the spectra obtained in argon and xenon matrices in this spectral region, in particular the different relative intensity of the bands at 1251 cm^{-1} (in argon) and 1249 cm^{-1} (in xenon), ascribable to conformer **II**, compared with the neighbor bands ascribable to conformer **I**, clearly reveal that both conformers **I** and **II** are present in the matrix.

Very interestingly, compared with the simulated spectrum, the intensity of the νC–O stretching band of form **II** appears larger in

the experimental spectra in relation to both the νC–O stretching band of form **I** and that assigned to νC$_{14}$–C$_{16}$ stretching mode (which, as stated above, has also a predominant contribution of this latter conformer). Furthermore, the relative intensification of the band due to conformer **II** is greater in the spectrum obtained in xenon than in argon (see Fig. 2). These observations cannot be interpreted as an indication of partial conversion of **I** into **II** during deposition of the matrices, since the calculated barrier is large enough to prevent this isomerization and, more importantly, if any isomerization between these two conformers could take place (e.g., in case the isomerization barriers in the matrices were much

smaller than in gas phase), this would have to occur exactly in the opposite direction, i.e., the less stable conformer **II** would have to be converted into the most stable form **I**. Moreover, this hypothetical conversion would have to occur in larger extent during deposition of the xenon matrix than during deposition of the argon matrix, both because xenon is well-known to be a better matrix medium for conformational cooling to take place than argon, and because the temperature of the cold window of the cryostat was kept at a higher temperature in the xenon experiments than in the argon ones.[51,75,76–80] Experimental observations show exactly the opposite trend, thus requiring a different explanation.

According to the calculations, the C–O ester bond is highly polarized in both conformers (see Table 2). However, it is considerably more polarized in conformer **II**, since the positive charge in the C_7 is larger in this form and the charge in O_9 is also more negative in conformer **II** than in **I**. These results are in agreement with the calculated relative infrared intensities of the νC–O bands: intense bands are predicted for this mode in both conformers, but the intensity in conformer **II** (595.2 km mol^{-1}) is almost twice that in conformer **I** (324.0 km mol^{-1}). This means that the C–O ester bond in **II** is also more sensitive to the polarizability of the media than the same bond in conformer **I**, being additionally polarized in greater extent in more polarizable media. Consequently, the relative infrared intensities of the νC–O stretching modes in conformer **II** compared to form **I** can be expected to grow in the order: gas phase<argon matrix<xenon matrix, as observed experimentally.

Assignment of a few other less intense bands to a single conformer was also attempted and is presented in Table 3, but they must be considered as tentative, e.g., bands ascribed uniquely to the less stable conformer (**II**) at 1461 (δCH_3 as′), 1047 [phenyl ring stretching vibration ($\delta Ph5$, as defined in Table S2) mixed with $\nu(C_1–C_{14})$], 906 [$\nu(C–Cl)$] and 659 cm^{-1} [$\delta(NNN)$] in argon, which in xenon appear at 1455/1453, 1045, 906, and 660/659 cm^{-1}, respectively.

3.3. Photochemistry of matrix-isolated MACBP

Upon in situ broadband UV irradiation (λ >235 nm) of matrix-isolated monomeric MACBP, a significant decrease in the intensity of the bands of the compound was observed, while new bands due to photoproducts emerged. These changes were already clearly visible after 10 min of irradiation, whereas more than 90% of the original compound was consumed after 450 min of irradiation of both argon and xenon matrices (see Experimental section for methodology used in the matrix isolation experiments). Analysis of the kinetic profiles of the bands appearing upon photolysis provided essentially two distinct patterns: (a) a set of bands starting to grow in the early stages of irradiation and then decreasing of intensity, and (b) the remaining bands starting to noticeably increase of intensity later on and in a continuous way. This behavior is shown in Fig. 3, which presents the infrared difference spectrum of the irradiated argon matrix of MACBP obtained subtracting the spectrum after 10 min of irradiation from that collected after 90 min of irradiation (before subtraction, residual bands due MACBP were subtracted from the spectra of the irradiated matrix). Bands pointing down in this spectrum correspond to the initially formed species, while those pointing up are due to photoproducts appearing at later stages of irradiation. Results obtained upon irradiation of the xenon matrix were qualitatively identical (see Fig. S3 in the Supplementary data).

It can be seen in both Fig. 3 and Fig. S3 that the spectrum of the initially predominant photoproduct fits well that theoretically predicted for the postulated azirine, methyl 2-benzoyl-2-chloro-2H-azirine-3-carboxylate (**2**, MBCAC). As already mentioned, these bands first start to grow and then considerably decrease for longer time of irradiation, indicating subsequent reactions of the 2H-
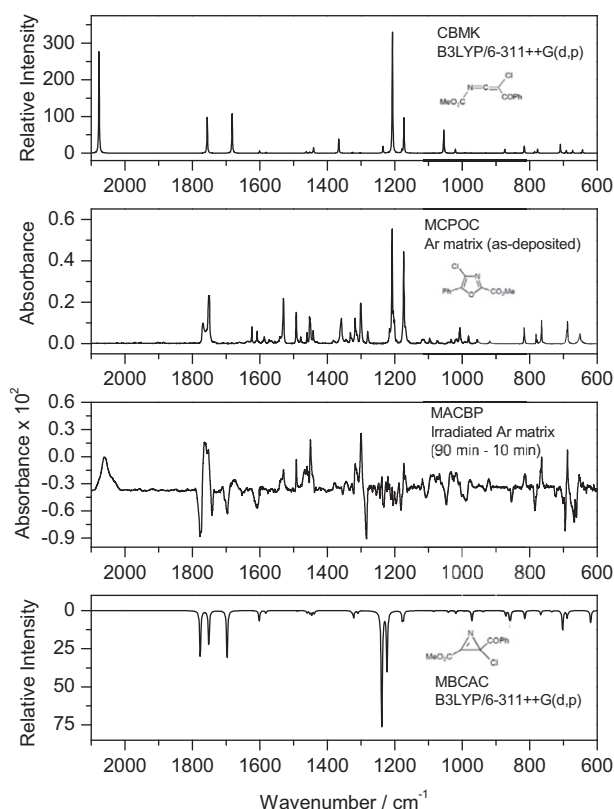

Fig. 3. *Top*: Simulated IR spectrum of CBMK (most stable conformer); *Middle top*: IR spectrum of MCPOC in argon matrix (as deposited; 10 K); *Middle bottom*: IR difference spectrum of irradiated Ar matrix of MACBP (λ >235 nm irradiated matrix during 90 min minus λ >235 nm irradiated matrix during 10 min; before subtraction, residual bands due MACBP were subtracted from the spectra of the irradiated matrix); *Bottom*: simulated IR spectrum of MBCAC (most stable conformer). In the simulated spectra, bands were represented by Lorenztian functions centered at the DFT(B3LYP)/6-311++G(d,p) calculated wavenumbers (scaled by 0.978) and with fwhm (full width at half maximum) equal to 2 cm^{-1} (in case of MBCAC, the spectrum was multiplied by −1).

azirine. On the other hand, the bands corresponding to the species detected later on are continuously growing with time of irradiation and fit well with those of methyl 4-chloro-5-phenyl-1,3-oxazole-2-carboxylate (**6**, MCPOC) and ketenimine **7** (CBMK) (see Scheme 2). In Fig. 4, the 1300–1150 cm^{-1} region of the spectrum of the as-deposited argon matrix of MACBP and of the spectra obtained for the irradiated matrix at two different times of irradiation is presented. This spectral range is crowded and contains strong overlapping absorptions of the reactant as well as of photoproducts, so that in the difference spectra shown in Fig. 3 a reliable analysis cannot be done. However, the data shown in Fig. 4 points to the same conclusions withdrawn from the general analysis of the spectral data presented in Fig. 3.

These observations can be rationalized considering that the oxazole derivative is a photoproduct of 2H-azirine **2** resulting from ring expansion via nitrile ylide intermediate **5**. On the other hand, the experimental results also indicate that ketenimine **7** must be formed from the starting 3-azido-acrylophenone **1**. In fact, the conversion of the 2H-azirine into ketenimine **7** would require the generation of vinyl nitrene **3**, which should also lead to its cyclization to the corresponding isoxazole. No formation of the isoxazole derivative was observed upon photolysis, which supports the conclusion[40] that the vinyl nitrene species is not involved in the generation of ketenimine **7**. With all probability this species is obtained from the starting azide via a Curtius type concerted rearrangement. Thus, the formation of 2H-azirine **2** and ketenimime **7** are competitive processes, being the former a kinetically
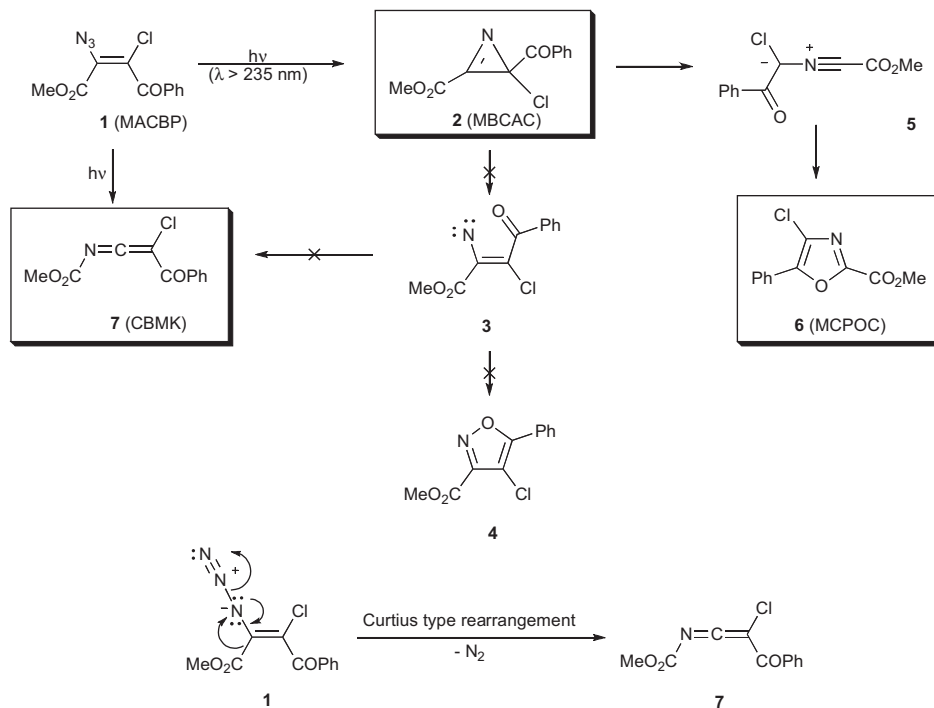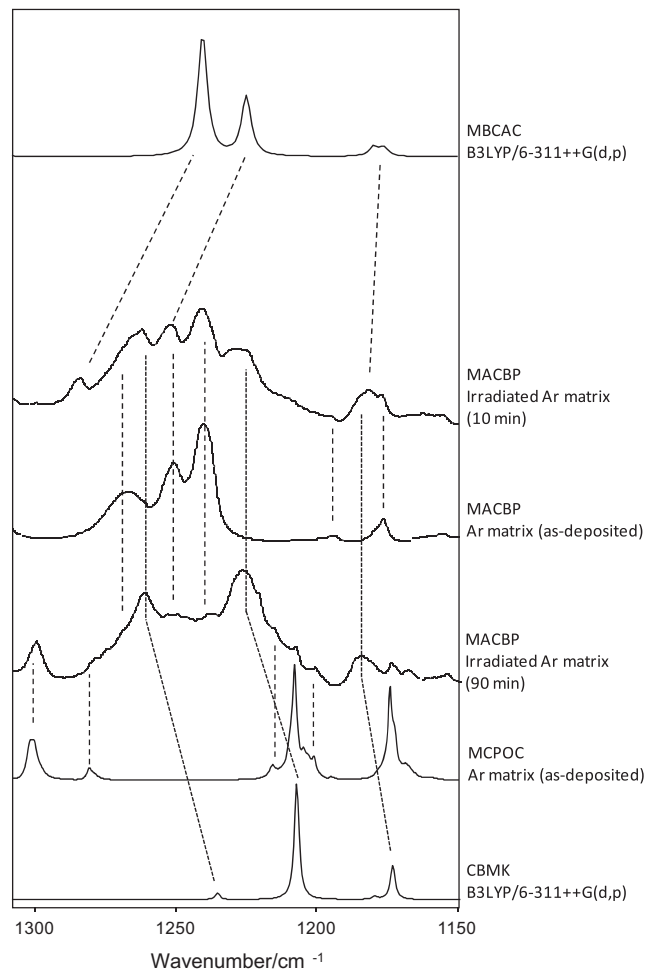
Scheme 2.

Fig. 4. *From top to bottom*: IR spectra (1300−1150 cm^{-1} region) of MBCAC (calculated; most stable conformer), MACBP (experimental, 10 K: λ >235 nm irradiated Ar matrix of the compound for 10 min, as-deposited Ar matrix, and λ >235 nm irradiated Ar matrix of the compound for 90 min), MCPOC (as-deposited Ar matrix; 10 K), and CBMK (calculated; most stable conformer). In the simulated spectra, bands were represented by Lorentzian functions centered at the DFT(B3LYP)/6-311++G(d,p) calculated wavenumbers (scaled by 0.978) and with fwhm (full width at half maximum) equal to 2 cm^{-1}.

Table 4
Vibrational assignments of the bands observed in the UV irradiated matrices of MACBP[a]

Irradiated **1** (MACBP) Ar matrix	Irradiated **1** (MACBP) Xe matrix	Experimental[81] or calculated data		Approximate description[b]
6 (MCPOC)		Ar matrix	Xe matrix	
ν	ν	ν	ν	
1764/1760/1753	1763/1758/1751	1769/1763/1751/1750	1763/1759/1748	ν(C=O)
1541/1536/1530	1537	1541/1530	1535/1532/1529	νOx1
1492	1490/1488	1492/1487	1489	δ(C–H2)
1478/1472	1474	1479	1478/1474	δCH$_3$ as'
1456	1456	1460	1455	δCH$_3$ as''
1450	1451/1448	1453/1452/1451/1450	1450/1444	δ(C–H3)
1447	1443	1442	1439/1436	δCH$_3$ s
1360/1358	1364/1340	1360/1358/1346	1361/1341	δ(C–H1); νPh2
1317/1313/1300	1313/1310/1298	1332–1300	1330–1302	νOx2; ν(C–C$_\alpha$)
1226–1198	1223/1199	1215–1202	1213–1197	ν(C–C$_{IR}$); ν(C–O); γCH$_3$'
1173/1168	1171/1163	1174/1172/1168/1166	1174/1170/1168/1163	γCH$_3$'; ν(C–O)
1118	1114	1117	1118/1114/1110/1109	νOx5
1093/1085	1089	1096/1094	1095/1092/1090	νPh6
1034	1034	1041/1033	1038/1031/1027	νPh5
1018/1008	1015/1006	1020/1016/1008/1006	1016/1007/1005	δOx1
977	977	981	980	νPh1
814	813	817/815	815/512	δ(OCO)
778	776	781/778	778/775	γ(C=O)
765	762	765	762	γ(C–H1)
690		691	690	δPh3
688	686	689/688/687	686	τOx1
653	651	652	650/648	τOx2
2 (MBCAC)		Calculated		
ν	ν	ν^c	I	
1776	1772	1777	188.4	ν(C=N) A
1742	1740	1752	144.7	ν(C=O) E
1706/1696	1694	1697	193.8	ν(C=O)
1608	1604	1602	42.6	νPh
	1584	1582	11.0	νPh
1464	1463	1460	9.5	δCH$_3$ as''
1454	1454	1452	11.3	δCH$_3$ as'
1444	1442	1446	18.2	δ(C–H) Ph
1438	1432	1439	12.8	δCH$_3$ s
1322	1320	1322	29.8	ν(C–C) A
1285	1283/1270/1262	1239	501.6	ν(C–C$_{Ph}$)
1254/1244/1234	1251/1236/1232	1223	244.3	ν(C–O)
1195	1194.	1178	38.2	δ(C–H) Ph
1181	1175	1174	32.8	γCH$_3$'
1047	1045	1041	7.3	ν(C–C(=O)); δ(C–H) Ph
1029/1025	1027/1021	1019	11.9	δPh
990	975	971	44.9	ν(O–CH$_3$)
862		871	20.3	ν(C–N) A
854	854	858	70.6	ν(C–Cl)
	819	815	33.0	δ(OCO)
785/773	784/771	767	17.7	γA–E
724	724	735	4.8	γ(C=O) E
702/694	694	702	81.1	γ(C–H) Ph
668/661	667/660	689	29.5	δPh
	623	619	51.1	δ(CC=O)
7 (CBMK)		Calculated		
ν	ν	ν^c	I	
2059	2055	2077	875.3	νC=C=N as
1764	1763	1756	311.6	ν(C=O) E
1680	1685	1682	350.9	ν(C=O)
	1588	1601	19.5	νPh
1440	1440	1441	45.7	δCH$_3$ s
1378	1366	1366	123.2	νC=C=N s
1238	1242	1235	56.7	ν(C–C$_{Ph}$)
[d]	[d]	1207	1042.2	ν(C–O)
1187	1184/1178	1173	304.8	γCH$_3$'
1067		1055	198.1	ν(C–C(=O)); δ(C–H) Ph
	823	816	60.3	ν(C–Cl)
718/711	715/708	709	76.9	γ(C–H) Ph
680	678	673	23.5	δPh
643	643	643	28.7	δ(CC=O); γ(C=C=N)

[a] Wavenumbers (ν) in cm^{-1} calculated intensities (**I**) in km mol^{-1}, ν, bond stretching, δ, bending, γ, rocking, τ, torsion, s, symmetric, as, asymmetric, Ox, oxazole ring, Ph, phenyl ring, A, azirine ring; E, ester, IR, inter-rings.
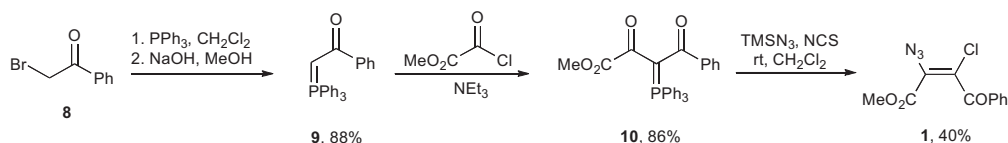[b] Approximate descriptions for MCPOC as in Ref. 83.
[c] Scaled wavenumbers (0.978).
[d] Buried within the profile due to MCPOC bands.

more favorable process, since at a shorter time of irradiation 2H-azirine dominates.

The assignments of the bands due to the photoproducts are presented in Table 4. It is worth mentioning that the spectrum of the photoproduced oxazole (MCPOC) in both argon and xenon matrices is well-known,[40,81] so that the identification of this compound in the irradiated MACBP matrices was doubtless and band assignment followed that presented before.[81] For example, bands at 1764/1760, 1753, 1541/1536/1530, 1492, 1300, and 1173/1168 cm^{-1}, in argon, with counterparts at 1763/1758, 1751, 1537, 1490/1488, 1298, and 1171/1163 cm^{-1}, in xenon, respectively, are intense characteristic bands of MCPOC.[81] On the other hand, for both the azirine and ketenimine species no experimental data for the matrix-isolated compounds were reported hitherto, so that their identification and band assignments were based on the comparison with theoretically predicted spectra obtained at the DFT(B3LYP)/6-311++G(d,p) level of theory and on data for other molecules of the same families.[47,50,51,82–91] Moreover, these two compounds have conformationally flexible molecules and, according to the structural calculations performed on these species, several low energy conformers exist in both cases. For the azirine, the calculations predicted the existence of five different conformers with relative energies within 10 kJ mol^{-1}. In the case of the ketenimine, the calculations yielded seven conformers with relative energies within the same limit. Nevertheless, the calculated infrared spectra of all low energy forms predicted theoretically for each molecule were found to be quite similar, thus facilitating their experimental identification and band assignments. Fig. 3 (and Fig. S3, in Supplementary data) shows only the spectra corresponding to the most stable conformer of each molecule, MBCAC and CBMK (see Fig. S4 for structures of these forms and Fig. S5 for the calculated spectra of CBMK and the nitrile ylide shown as stick spectra), while the calculated data for these molecules shown in Table 4 also belong only to their most stable forms.

Among the bands ascribed to MBCAC (see Table 4) the most intense ones were observed at 1776, 1742, 1706/1696, 1608, 1285, 702/694, and 668/661 cm^{-1} in argon (1772, 1740, 1694,1604, 1283/1270/1262, 694, and 667/660 cm^{-1} in xenon), corresponding to the ν(C=N) stretching of the azirine ring, ν(C=O) stretchings in ester and benzoyl fragments, the highest frequency stretching mode of the phenyl group, the stretching vibration of the C–C$_{Ph}$ bond, and the all in phase rocking out-of-plane C–H deformation and a skeletal deformational mode of the phenyl group, which were predicted to occur at 1777, 1752, 1697, 1602, 1239, 702, and 689 cm^{-1}, respectively. The most characteristic band of CBMK was observed at 2059 cm^{-1} (argon) and 2055 (xenon) cm^{-1}, and is ascribed to the ketenimine νC=C=N anti-symmetric stretching mode.[48–51,54,55]

MACBP, the presence of such band could not be confirmed (see Fig. S5 for the calculated spectrum of nitrile ylide 5).

4. Conclusions

The 3-azido-acrylophenone MACBP (or methyl (Z)-2-azido-3-chloro-3-benzoyl-propenoate) has been shown to be a photochemical precursor of the related oxazole, methyl 4-chloro-5-phenyl-1,3-oxazole-2-carboxylate (MCPOC), in a reaction where the azirine and nitrile ylide work as intermediates. This reaction is accompanied by a second one leading to formation of C-chloro-C-benzoyl-N-methoxycarbonylketenimine (CBMK) via a Curtius type concerted rearrangement of the starting 3-azido-acrylophenone 1. The alternative mechanistic pathway involving the initial formation of the 2H-azirine followed by the C–N bond cleavage giving a vinyl nitrene, which then rearranges to the ketenimine was ruled out. The non-observation of the isoxazole, the expected vinyl nitrene cyclization product, points to the concerted nature of ketenimine formation.

MACBP was synthesized, isolated in low temperature argon and xenon matrices and structurally and vibrationally characterized by infrared spectroscopy and quantum chemical calculations before execution of the photochemical studies. Seven different low energy conformers were found on the DFT(B3LYP)/6-311++G(d,p) PES, with the three lower energy forms (which correspond to the conformers predicted to have significant populations in the gas phase equilibrium at the sublimation temperature required to produce the cryogenic matrices) showing an orientation of the azide group in a nearly trans orientation. In the matrix isolation experiments, however, only the two most stable conformers of the compound (I and II) were observed, in agreement with the predicted easy conversion of conformer III into conformer II during deposition of the matrices, due to the very low energy barrier associated with this conversion (ca. 0.03 kJ mol^{-1}).

5. Experimental section

5.1. Synthesis of MACBP

(Z)-3-Azido-3-methoxycarbonyl-2-chloro-acrylophenone (1) was prepared using a known synthetic method procedure (Scheme 3).[39] The 2-(triphenylphosphoranylidene)acetophenone (9), obtained by reaction of 2-bromoacetophenone 8 and triphenylphosphine, was added to a solution of triethylamine in dry toluene and treated with the appropriated acid chloride to give the methyl 2,4-dioxo-4-phenyl-3-triphenylphosphoranylidenebutanoate (10) almost in good yield. This ylide reacts with azidotrimethylsilane and N-chlorosuccinimide in dichloromethane to give the crystalline

Scheme 3. Synthesis of methyl (Z)-3-azido-acrylophenone 1.

In the present study, among the species predicted to take part in the azide→oxazole photochemical conversion (Scheme 2), only the nitrile ylide 5 could not be doubtlessly observed, indicating that for the system under study this species is a quite unstable intermediate, which is promptly converted to the oxazole. The intrinsically strong band in infrared due to the anti-symmetric stretching of the CN$^+$C$^-$ moiety of a nitrile ylide appears usually at a characteristic frequency of about 1950 cm^{-1}.[48,49,54,55] In both the infrared spectra of the photolyzed argon and xenon matrices of

target compound 1 after purification by column chromatography and crystallization.

5.2. Matrix isolation experiments

Matrices were prepared by co-deposition of MACBP vapors coming out from a specially designed thermoelectrically heatable mini-furnace, assembled inside the cryostat (APD Cryogenics, model DE-202A) chamber, and large excess of the matrix gas (argon, N60;

xenon, N48, both obtained from Air Liquide) onto a CsI substrate cooled to 10 K (for argon matrices) and 20 K (for xenon matrices). The IR spectra were recorded with 0.5 cm^{-1} spectral resolution in a Mattson (Infinity 60AR Series) Fourier transform infrared spectrometer, equipped with a deuterated triglycine sulfate (DTGS) detector and a Ge/KBr beam splitter. Necessary modifications of the sample compartment of the spectrometer were done in order to accommodate the cryostat head and allow purging of the instrument by a stream of dry nitrogen, to remove water vapors and CO_2.

Irradiation of the matrices was carried out with unfiltered light from a 500 W Hg(Xe) lamp (Newport, Oriel Instruments), with output power set to 200 W, through the outer KBr windows of the cryostat (λ >235 nm).

Acknowledgements

Supplementary data

Additional figures with schematic schematic representations of the four higher energy conformers of MACBP and the low energy conformers of MBCAC and CBMK, predicted IR spectra for the three conformers of MBCAC, CBMK and nitrile ylide, and spectral data showing the observed in xenon matrix photochemistry are provided as Supplementary data. Also, tables with optimized geometries, IR spectroscopic data of three most stable, experimentally relevant conformers of MACBP (forms **I**, **II** and **III**), and Cartesian coordinates and absolute energies for the relevant forms calculated and discussed. Supplementary data associated with this article can be found, in the online version, at doi:10.1016/j.tet.2011.07.084.

References and notes

1. *Organic Azides, Syntheses and Applications*; Bräse, S., Baneet, K., Eds.; John Wiley: UK, 2010.
2. *The Chemistry of the Azido Group*; Patai, S., Ed.; Wiley: New York, NY, 1971.
3. Scriven, E. F. V.; Turnbull, K. *Chem. Rev.* **1988**, *88*, 297.
4. Bräse, S.; Gil, C.; Knepper, K.; Zimmerman, V. *Angew. Chem., Int. Ed.* **2005**, *44*, 5188.
5. Fotsing, J. R.; Banert, K. *Synthesis* **2006**, *2*, 261.
6. Maurus, R.; Bogumil, R.; Nguyen, N. T.; Mauk, A. G.; Brayer, G. *Biochem. J.* **1998**, *332*, 67.
7. Canalle, L. A.; Löwik, D. W. P. M.; Hest, J. C. M. *Chem. Soc. Rev.* **2010**, *39*, 329.
8. Pathak, T. *Chem. Rev.* **2002**, *102*, 1623.
9. Greenberg, W. A.; Priestley, E. S.; Sears, P. S.; Alper, P. B.; Rosenbohm, C.; Hendrix, M.; Hung, S.-C.; Wong, C.-H. *J. Am. Chem. Soc.* **1999**, *121*, 6527.
10. Hein, C. D.; Liu, X.-M.; Wang, D. *Pharm. Res.* **2008**, *25*, 2216.
11. Colombo, M.; Peretto, I. *Drug Discovery Today* **2008**, *13*, 678.
12. Reddy, N. N.; Mohan, Y. M.; Varaprasad, K.; Ravindra, S.; Vimala, K.; Raju, K. M. *J. Appl. Polym. Sci.* **2010**, *115*, 1589.
13. Lakshmi, S.; Kumar, S. S.; Jayakrishnan, A. *J. Biomed. Mater. Res.* **2002**, *61*, 26.
14. Nájera, C.; Sansano, J. M. *Org. Biomol. Chem.* **2009**, *7*, 4567.
15. Huisgen, R. In *1,3-Dipolar Cycloaddition Chemistry*; Padwa, A., Ed.; Wiley: New York, NY, 1984; Vol. 1, pp 1–176.
16. Lutz, J.-F. *Angew. Chem., Int. Ed.* **2007**, *46*, 1018.
17. Binder, W. H.; Sachsenhofer, R. *Macromol. Rapid Commun.* **2008**, *29*, 952.
18. Himo, F.; Lovell, T.; Hilgraf, R.; Rostovtsev, V. V.; Noodleman, L.; Sharpless, K. B.; Fokin, V. V. *J. Am. Chem. Soc.* **2005**, *127*, 210.
19. Nulwala, H.; Burke, D. J.; Khan, A.; Serrano, A.; Hawker, C. J. *Macromolecules* **2010**, *43*, 5474.
20. Dabbagh, A. H.; Mansoori, Y. *Dyes Pigm.* **2002**, *54*, 37.
21. Yan, M.; Cai, S. X.; Wybourne, M. N.; Keana, J. F. W. *J. Am. Chem. Soc.* **1993**, *115*, 814.
22. Nahar, P.; Wali, N. M.; Gandhi, R. P. *Anal. Biochem.* **2001**, *294*, 148.
23. Cai, S. X.; Glenn, D. J.; Kanskar, M.; Wybourne, M. N.; Keana, J. F. W. *Chem. Mater.* **1994**, *6*, 1822.
24. Tattersall, P. I.; Breslin, D.; Grayson, S. M.; Heath, W. H.; Lou, K.; McAdams, C. L.; McKean, D.; Rathsack, B. M.; Willson, C. G. *Chem. Mater.* **2004**, *16*, 1770.
25. Fleming, S. A. *Tetrahedron* **1995**, *51*, 12479.
26. Ballell, L.; Alink, K. J.; Slijper, M.; Versluis, C.; Liskamp, R. M. J.; Pieters, R. J. *ChemBioChem* **2005**, *6*, 291.
27. Kubota, N. *J. Propul. Power* **1995**, *11*, 677.
28. Badgujar, D. M.; Talawar, M. B.; Asthana, S. N.; Mahulikar, P. P. *J. Hazard. Mater.* **2008**, *151*, 289.
29. L' Abbé, G. *Chem. Rev.* **1969**, *69*, 345.
30. Hassner, A. In *Azides and Nitrenes. Reactivity and Utility*; Scriven, E. F. V., Ed.; Academic: Orlando, 1984.
31. Platz, M. S. *Acc. Chem. Res.* **1995**, *28*, 487.
32. Wentrup, C. *Top. Curr. Chem.* **1976**, 175.
33. Hassner, A.; Fowler, F. W. *J. Am. Chem. Soc.* **1968**, *90*, 2869.
34. Hassner, A.; Wiegand, N. H.; Gottlieb, H. E. *J. Org. Chem.* **1986**, *51*, 3176.
35. Morawietz, J.; Sander, W. *J. Org. Chem.* **1996**, *61*, 4351.
36. Dyke, J. M.; Levita, G.; Morris, A.; Ogden, J. S.; Dias, A. A.; Algarra, M.; Santos, J. P.; Costa, M. L.; Rodrigues, P.; Barros, M. T. *J. Phys. Chem. A* **2004**, *108*, 5299.
37. Bock, H.; Damme1, R. *J. Am. Chem. Soc.* **1988**, *110*, 5261.
38. Gritsan, N. P. *Russ. Chem. Rev.* **2007**, *76*, 1139.
39. Pinho e Melo, T. M. V. D.; Lopes, C. S. J.; Cardoso, A. L.; d'A. Rocha Gonsalves, A. M. *Tetrahedron* **2001**, *57*, 6203.
40. Lopes, S.; Nunes, C. M.; Fausto, R.; Pinho e Melo, T. M. V. D. *J. Mol. Struct.* **2009**, *919*, 47.
41. Pinho e Melo, T. M. V. D.; Lopes, C. S. J.; d'A Rocha Gonsalves, A. M.; Storr, R. C. *Synthesis* **2002**, *5*, 605.
42. Padwa, A.; Smolanoff, J.; Temper, A. *J. Org. Chem.* **1976**, *41*, 543.
43. Padwa, A.; Smolanoff, J.; Temper, A. *J. Am. Chem. Soc.* **1975**, *97*, 1945.
44. Isomura, K.; Ayabe, G.-I.; Hatano, S.; Taniguchi, H. *J. Chem. Soc., Chem. Commun.* **1980**, 1252.
45. Wendling, L. A.; Bergman, R. G. *J. Org. Chem.* **1976**, *41*, 831.
46. Singh, B.; Zweig, J.; Gallivant, J. B. *J. Am. Chem. Soc.* **1972**, *94*, 1199.
47. Orton, E.; Collins, S. T.; Pimentel, G. C. *J. Phys. Chem.* **1986**, *90*, 6139.
48. Inui, H.; Murata, S. *J. Am. Chem. Soc.* **2005**, *127*, 2628.
49. Inui, H.; Murata, S. *Chem. Lett.* **2001**, *30*, 832.
50. Kaczor, A.; Gómez-Zavaglia, A.; Cardoso, A. L.; Pinho e Melo, T. M. V. D.; Fausto, R. *J. Phys. Chem. A* **2006**, *110*, 10742.
51. Gómez-Zavaglia, A.; Kaczor, A.; Cardoso, A. L.; Pinho e Melo, T. M. V. D.; Fausto, R. *J. Phys. Chem. A* **2006**, *110*, 8081.
52. Bornemann, C.; Klessinger, M. *Chem. Phys.* **2000**, *259*, 263.
53. Klessinger, M.; Bornemann, C. *J. Phys. Org. Chem.* **2002**, *15*, 514.
54. Inui, H.; Murata, S. *Chem. Commun.* **2001**, 1036.
55. Inui, H.; Murata, S. *Chem. Phys. Lett.* **2002**, *359*, 267.
56. Stewart, J. J. P. *J. Comput. Chem.* **1989**, *10*, 209.
57. Stewart, J. J. P. *J. Comput. Chem.* **1989**, *10*, 221.
58. HyperChem Conformational Search module *Tools for Molecular Modeling*; Hypercube: 1115 NW 4th St., Gainesville, FL 32608 (USA), 2002.
59. Saunders, M. *J. Am. Chem. Soc.* **1987**, *109*, 3150.
60. Saunders, M.; Houk, K. N.; Wu, Y.-D.; Still, W. C.; Lipton, J. M.; Chang, G.; Guidal, W. C. *J. Am. Chem. Soc.* **1990**, *112*, 1419.
61. Howard, A. E.; Kollman, P. A. *J. Med. Chem.* **1988**, *31*, 1669.
62. Frisch, M. J.; Trucks, G. W.; Schlegel, H. B.; Scuseria, G. E.; Robb, M. A.; Cheeseman, J. R.; Montgomery, J. A., Jr.; Vreven, T.; Kudin, K. N.; Burant, J. C.; Millam, J. M.; Iyengar, S. S.; Tomasi, J.; Barone, V.; Mennucci, B.; Cossi, M.; Scalmani, G.; Rega, N.; Petersson, G. A.; Nakatsuji, H.; Hada, M.; Ehara, M.; Toyota, K.; Fukuda, R.; Hasegawa, J.; Ishida, M.; Nakajima, T.; Honda, Y.; Kitao, O.; Nakai, H.; Klene, M.; Li, X.; Knox, J. E.; Hratchian, H. P.; Cross, J. B.; Bakken, V.; Adamo, C.; Jaramillo, J.; Gomperts, R.; Stratmann, R. E.; Yazyev, O.; Austin, A. J.; Cammi, R.; Pomelli, C.; Ochterski, J. W.; Ayala, P. Y.; Morokuma, K.; Voth, G. A.; Salvador, P.; Dannenberg, J. J.; Zakrzewski, V. G.; Dapprich, S.; Daniels, A. D.; Strain, M. C.; Farkas, O.; Malick, D. K.; Rabuck, A. D.; Raghavachari, K.; Foresman, J. B.; Ortiz, J. V.; Cui, Q.; Baboul, A. G.; Clifford, S.; Cioslowski, J.; Stefanov, B. B.; Liu, G.; Liashenko, A.; Piskorz, P.; Komaromi, I.; Martin, R. L.; Fox, D. J.; Keith, T.; Al-Laham, M. A.; Peng, C. Y.; Nanayakkara, A.; Challacombe, M.; Gill, P. M. W.; Johnson, B.; Chen, W.; Wong, M. W.; Gonzalez, C.; Pople, J. A. *Gaussian 03, revision C.02*; Gaussian: Wallingford, CT, 2004.
63. Frisch, M. J.; Head-Gordon, M.; Pople, J. A. *Chem. Phys. Lett.* **1990**, *166*, 281.
64. Becke, A. D. *Phys. Rev. A* **1988**, *38*, 3098.
65. Lee, C. T.; Yang, W. T.; Parr, R. G. *Phys. Rev. B* **1988**, *37*, 785.
66. Császár, P.; Pulay, P. *J. Mol. Struct.* **1984**, *114*, 31.
67. Farkas, Ö; Schlegel, H. B. *J. Chem. Phys.* **1999**, *111*, 10806.
68. Peng, C.; Schlegel, H. B. *Isr. J. Chem.* **1994**, *33*, 449.
69. Schachtschneider, J. H.; Mortimer, F. S. Vibrational Analysis of Polyatomic Molecules. VI. FORTRAN IV Programs for Solving the Vibrational Secular Equation and for the Least-Squares Refinement of Force Constants. Report No. 31450. Structural Interpretation of Spectra, Technical Report no 57-650, Shell Development. Emeryville, CA, 1969.
70. Pulay, P.; Fogarasi, G.; Pang, F.; Boggs, J. E. *J. Am. Chem. Soc.* **1979**, *110*, 2550.
71. Fausto, R.; Teixeira-Dias, J. J. C. *J. Mol. Struct.* **1986**, *144*, 215.
72. Fausto, R.; Teixeira-Dias, J. J. C. *J. Mol. Struct.* **1986**, *144*, 225.
73. Fausto, R.; Teixeira-Dias, J. J. C. *J. Mol. Struct.* **1986**, *144*, 241.
74. Cioslowski, J. *J. Am. Chem. Soc.* **1989**, *111*, 8333.
75. Barnes, A. J. *J. Mol. Struct.* **1984**, *113*, 161.
76. Reva, I. D.; Stepanian, S. G.; Adamowicz, L.; Fausto, R. *Chem. Phys. Lett.* **2003**, *374*, 631.
77. Gómez-Zavaglia, A.; Fausto, R. *J. Mol. Struct.* **2004**, *689*, 199.
78. Borba, A.; Gómez-Zavaglia, A.; Simões, P. N. N. L.; Fausto, R. *J. Phys. Chem. A* **2005**, *109*, 3578.
79. Rosado, M. T. S.; Lopes de Jesus, A. J.; Reva, I. D.; Fausto, R.; Redinha, J. S. *J. Phys. Chem. A* **2009**, *133*, 7499.
80. Reva, I. D.; Lopes de Jesus, A. J.; Rosado, M. T. S.; Fausto, R.; Eusùbio, M. E.; Redinha, J. S. *Phys. Chem. Chem. Phys.* **2006**, *8*, 5339.

81. Lopes, S.; Nunes, C. M.; Gómez-Zavaglia, A.; Pinho e Melo, T. M. V. D.; Fausto, R. *J. Phys. Chem. A* **2010**, *114*, 9074.
82. Finnerty, J.; Mitschke, U.; Wentrup, C. *J. Org. Chem.* **2002**, *67*, 1084.
83. Jacox, M. E.; Milligan, D. E. *J. Am. Chem. Soc.* **1963**, *85*, 278.
84. Jacox, M. E. *Chem. Phys.* **1979**, *43*, 157.
85. Guillemin, J.-C.; Denis, J.-M.; Lasne, M.-C.; Ripoll, J.-L. J. *Tetrahedron* **1988**, *44*, 4447.
86. Ripoll, J.-L.; Thuillier, A. *Tetrahedron Lett.* **1978**, 463.
87. De Corte, B.; Denis, J.-M.; De Kimpe, N. *J. Org. Chem.* **1987**, *52*, 1147.
88. Amatatsu, Y.; Hamada, Y.; Tsuboi, M. *J. Mol. Spectrosc.* **1987**, *123*, 476.
89. August, J.; Klemm, K.; Kroto, H. W.; Walton, D. R. M. *J. Chem. Soc., Perkin Trans. 2* **1989**, 1841.
90. Winter, H.-W.; Wentrup, C. *Angew. Chem.* **1980**, *92*, 743.
91. Winter, H.-W.; Wentrup, C. *Angew. Chem., Int. Ed. Engl.* **1980**, *19*, 720.